Smart Structures and Systems, *Vol. 30, No. 6 (2022) 583-599*
https://doi.org/10.12989/sss.2022.30.6.583

Wireless sensor network design for large-scale infrastructures health monitoring with optimal information-lifespan tradeoff

Xiao-Han Hao [1,2a], Sin-Chi Kuok [1,2b] and Ka-Veng Yuen*[1,2]

[1] *State Key Laboratory of Internet of Things for Smart City and Department of Civil and Environmental Engineering, University of Macau, Macao SAR, China*
[2] *Guangdong-Hong Kong-Macau Joint Laboratory for Smart Cities, University of Macau, Macao SAR, China*

(*Received March 31, 2022, Revised September 6, 2022, Accepted September 15, 2022*)

Abstract. In this paper, a multi-objective wireless sensor network configuration optimization method is proposed. The proposed method aims to determine the optimal information and lifespan wireless sensor network for structural health monitoring of large-scale infrastructures. In particular, cluster-based wireless sensor networks with multi-type of sensors are considered. To optimize the lifetime of the wireless sensor network, a cluster-based network optimization algorithm that optimizes the arrangement of cluster heads and base station is developed. On the other hand, based on the Bayesian inference, the uncertainty of the estimated parameters can be quantified. The coefficient of variance of the estimated parameters can be obtained, which is utilized as a holistic measure to evaluate the estimation accuracy of sensor configurations with multi-type of sensors. The proposed method provides the optimal wireless sensor network configuration that satisfies the required estimation accuracy with the longest lifetime. The proposed method is illustrated by designing the optimal wireless sensor network configuration of a cable-stayed bridge and a space truss.

Keywords: Bayesian inference; measurement information; multi-type sensor system; network lifespan; system identification; wireless sensor network

1. Introduction

Structural health monitoring (SHM) of large-scale infrastructures has been attracting tremendous interest over the recent decades (Lam *et al*. 2006, Lei *et al*. 2010, 2015, 2017, Noori *et al*. 2010, Casciati and Fuggini 2011, Lam *et al*. 2012, 2017, 2018, Yi *et al*. 2013, 2016, 2017, 2020, Zhang *et al*. 2016, Zhao *et al*. 2018, Spencer *et al*. 2019, Lam and Adeagbo 2022). In traditional SHM systems, the monitored data is collected using wired sensors and it is transmitted by cables from the sensor nodes to the base station. In recent years, due to deployment convenience and onboard computation, wireless sensor networks have been widely used in civil engineering (Jung *et al*. 2011, Fu *et al*. 2013). As the advanced sensing technology, wireless sensor eliminates the cost of wiring and improve the flexibility of SHM systems. The placement of wireless sensors is a critical issue in SHM because the monitoring locations affect the quality of the captured information. If the wireless sensor network is designed improperly, the performance of the identification results and thus the evaluation on the structural health condition can be seriously distorted. To ensure the identification performance of a sensor network, various methods have been proposed (Yao *et al*. 1993, Papadopoulos and Garcia 1998, Reynier and Abou-Kandil 1999, Gul and Catbas 2011, Stephan 2012, Yi *et al*. 2015, Li *et al*. 2017a, Pei *et al*. 2018, Argyris *et al*. 2018). The four major categories are response reconstruction-based approach (Yao *et al*. 1993), modal parameters-based approach (Reynier and Abou-Kandil 1999), energy-based approach (Papadopoulos and Garcia 1998) and information-based approach (Kammer 1991). In particular, the information-based approach provides a promising direction to address the sensor placement optimization problem (Kammer 1991, Udwadia 1994, Heredia-Zavoni and Esteva 1998, Raich and Liszkai 2012, Li *et al*. 2017b, Argyris *et al*. 2018, Shi *et al*. 2020). An effective independence method is presented for the optimal sensor placement design using the determinant of the Fisher information matrix (Kammer 1991). Heredia-Zavoni and Esteva (1998) minimized the expected value of a Bayesian loss function for selecting the optimal locations of sensors. Shi *et al*. (2020) proposed an eigenvector sensitivity method to obtain the optimal sensor placement based on the collected information. The information entropy (IE) is widely used to develop information-based sensor placement methods (Papadimitriou *et al*. 2000, Ye and Ni 2012, Argyris *et al*. 2017, Zhang *et al*. 2017). Papadimitriou (2004) proposed an entropy-based method to optimize the sensor placement. Yuen and Kuok (2015) presented an efficient IE-based method for designing the optimal placement of multi-type sensors. Yuen *et al*. (2022) introduced the robust IE to develop a robust sensor placement method for structural identification with possibly malfunctioning sensors based

*Corresponding author, Ph.D., Distinguished Professor,
E-mail: kvyuen@um.edu.mo
[a] Graduate Student
[b] Ph.D., Assistant Professor

ISSN: 1738-1584 (Print), 1738-1991 (Online)

on the robust IE.

The wireless sensor transmits data by radio, and it is commonly battery powered (Kurata *et al*. 2005, Al-Turjman 2018). Excessive energy consumption causes the early termination of the sensor node in the wireless network, and shortens its operation lifetime. Therefore, not only the estimation accuracy, but also the lifetime of the network should be considered when designing the optimal wireless sensor network configuration (Cho *et al*. 2008, Fu *et al*. 2013, Sengupta *et al*. 2013, Zhou and Yi 2013, Jalsan *et al*. 2014, Al-Turjman *et al*. 2015, Elsersy *et al*. 2016, El-Qawasma *et al*. 2019). Li *et al*. (2010) emphasized the importance of the lifetime of wireless sensor networks and reorganized the SHM mechanism to optimize the sensor placement. Onoufriou *et al*. (2012) took the information effectiveness and the energy efficiency into consideration to optimize both the number of sensors and the sensor locations. Bhuiyan and Cao (2015) designed the wireless sensor placement with consideration of the network robustness, communication efficiency and identification effectiveness. Zhou *et al*. (2015) investigated the wireless sensor placement optimization to improve the energy balance, network connectivity and the identification quality. Furthermore, various wireless sensor configuration optimization methods based on the cluster-based network is proposed (Liu *et al*. 2011, 2016, Fang *et al*. 2018, Geoffrine and Geetha 2019).

To establish a wireless sensor network, the cluster-based network is an effective routing to reduce the redundant data in the network based on the data aggregation technology (Wang *et al*. 2001). Liu *et al*. (2011) presented a cluster-based modal analysis strategy to improve the network performance of the wireless sensor network. An optimal cluster-based network for the heterogeneous wireless sensors is developed to maintain good energy efficiency of the network (Liu *et al*. 2016). Fang *et al*. (2018) selected the optimal cluster-based wireless sensor network configuration by determining the optimal number of clusters in the network. Geoffrine and Geetha (2019) determined the optimal locations for wireless sensors by exhaustive search, and then designed the optimal wireless network for the deployed sensor nodes.

The aforementioned cluster-based wireless sensor network configuration methods focused on the optimization of the total energy consumption of the wireless network without considering the energy consumption of single sensor node. In practice, excessive energy consumption of a node will fasten the energy draining of its battery and affect the completeness of the monitoring locations of a wireless network. On the other hand, a fixed base station is assumed in most existing methods for cluster-based wireless sensor network configuration optimization. However, the energy consumed by the sensors varies with the location of the base station (Akkaya *et al*. 2007). The sensor nodes with shorter distances to the base station were assigned to be the cluster head nodes. The non-cluster head node transmitted data to one of these cluster head nodes. Consequently, the cluster head nodes may have high energy consumption due to overload. In this study, a cluster-based network optimization algorithm with consideration of the energy consumption is presented. It optimizes the locations of the cluster head and base station such that the network configuration with longest lifespan can be established.

In this paper, a multi-objective versatile wireless sensor network configuration optimization method is presented. It is an information-based method and cluster-based routing is considered. Bayesian inference is utilized to quantify the uncertainty of the estimated parameters. The estimation accuracy of the sensor placement is evaluated based on the coefficient of variance (COV) of the estimated parameters. The proposed method develops the maximum lifespan wireless sensor network configuration that satisfies the required estimation accuracy. Furthermore, we present a bio-inspired iterative optimization procedure to reduce the computational cost in establishing the optimal design.

This paper is organized as follows. Section 2 describes the concerned multi-objective wireless sensor network configuration design problem. In Section 3, the proposed cluster-based network optimization algorithm is presented. Section 4 presents the formulation for structural identification. Section 5 summarizes the procedure of the proposed method. In Section 6, the performance of the proposed method is demonstrated with two illustrative examples. The first example refers to a cable-stayed bridge while the second example refers to a space truss.

2. Problem description

In this study, we propose a multi-objective optimal wireless sensor network configuration algorithm to optimize the network operation lifespan while guarantee the measurement information for continuous structural health monitoring (SHM). The lifespan of wireless sensor network refers to the monitoring period till the battery of a sensor runs out of energy. It can cause the data loss of one sensor channel or even the termination of data transmission of the neighboring sensors. The lifespan is optimized so that the network can function properly for the longest time. On the other hand, we present the coefficient of variation (COV) of the estimated parameters to quantify the information quality of sensor configuration. The goal of this work is to develop the optimization method so that the network can operate with maximum lifetime while the identified parameters can achieve the required estimation accuracy.

Consider a dynamical system with N_d degree of freedoms (DOFs) and N_m structural members, a wireless sensor network with $N_{\mathcal{T}}$ types of sensors are utilized to monitor the structural response. Assume that the network contains N_τ sensors for the type τ sensor. The sensor location of the νth sensor of the type τ sensor is given by $s_{\tau,\nu} \in \boldsymbol{\mathcal{P}}_\tau$, where $\boldsymbol{\mathcal{P}}_\tau$ is a set of possible locations for the τth type of sensor. For displacement transducer, velocity transducer and accelerometer, the possible locations are equal to N_d while for strain gauge, the possible locations are equal to N_m. Therefore, the locations of all deployed sensors in the wireless sensor network can be expressed as $\mathbf{S} = \{s_{\tau,\nu} | \tau = 1,2,\dots,N_{\mathcal{T}}, \nu = 1,2,\dots,N_\tau\}$. The total number of sensors in the network is $N_s = \sum_{\tau=1}^{N_{\mathcal{T}}} N_\tau$.

Let $\mathbf{W_S}$ to denote the routing configuration of the wireless sensor network based on the deployed wireless

sensors with $\mathbf{S}$. It describes the cluster-based routing for data transmission between the sensors and the base station. The wireless sensors are grouped into clusters. Each cluster contains one single type of sensors and one of the sensors is selected as the cluster head node while the rest are the non-cluster head nodes. The cluster head is responsible to transfer the measurements from all sensors in the cluster to the base station. Each sensor node has a battery with a stored energy ε_0. The sensor node that consumes the largest amount of energy among all sensor nodes in $\mathbf{W_S}$ during one round of data collection will first run out of energy. The rate of energy consumption is denoted as $E_{\mathcal{M}}(\mathbf{W_S})$ and this node is regarded as the dominated sensor node of the network $\mathbf{W_S}$. Therefore, the lifetime of the network indicates the total rounds of data collection before the dominated sensor node has run out of energy. The lifetime of the wireless sensor network with routing configuration $\mathbf{W_S}$ defined as the ratio between the stored energy and the rate of energy consumption of the dominated sensor node (Mak and Seah 2009)

$$L(\mathbf{W_S}) = \frac{\varepsilon_0}{E_{\mathcal{M}}(\mathbf{W_S})} \tag{1}$$

Herein, the stored energy ε_0 is restricted by the inherent battery properties. To maximize the lifetime of the wireless sensor network, we aim to design the network configuration such that $E_{\mathcal{M}}(\mathbf{W_S})$ can be minimized without deteriorating the quality of measurement information.

To quantify the quality of measurement information, the estimation accuracy of the identified structural parameters is evaluated. In particular, Bayesian inference is implemented to compute the coefficient of variation (COV) of the estimates (Yuen and Kuok 2015, Yuen *et al*. 2022). On the other hand, the consumed energy at a sensor node depends on the wireless sensor network configuration, such as, the design of the clusters, the selection of the cluster head nodes, the data transmission paths, etc. Therefore, the optimal design of the wireless network configuration is the one that can maximize the lifetime of the network (or equivalently, minimize the rate of energy consumption of the dominated sensor node) while satisfy the accuracy requirement.

In a sensory system, if the sensors are closely distributed, the neighboring sensors may provide overlapped information and the captured information about the structure can be incomplete. On the contrary, if the sensors are distributed sparsely, overall information about different regions of the structure can be monitored. However, the consumed energy for data transmission will increase and shorten the lifetime of the network. The optimal information-lifespan provides the tradeoff between the captured information from the sensing devices and the operation lifespan of the battery-powered wireless network. Based on the limited sensing devices, a more informative configuration tends to have a more widespread arrangement. However, a longer lifetime implies lower operation energy with shorter transmission distances between the network components. The resultant optimal configuration takes the best tradeoff so that the estimation accuracy can be satisfied with the longest operation lifespan. To achieve the best trade-off between the information gain and lifetime, the sensor placement optimization problem is formulated as follows

$$\max_{\mathbf{S}} L(\mathbf{W_S^*}) \quad \text{subject to} \quad \xi_{\mathbf{S},\mathcal{M}} < \xi_r \tag{2}$$

where $\mathbf{W_S^*}$ is the optimal network configuration regarding the sensor locations $\mathbf{S}$; $\xi_{\mathbf{S},\mathcal{M}}$ is the maximum COV of the estimated parameters obtained by the sensors with $\mathbf{S}$; and ξ_r is the required COV threshold of the estimated parameter. The required COV threshold of the estimated parameters is a user-specified quantity that depends on the acceptable estimation uncertainty tolerance and the limitation of the hardware. If a specified threshold cannot be fulfilled, an increased number of sensing devices and/or higher resolution transceivers should be introduced. Otherwise, a higher COV threshold tolerance (i.e., lower estimation accuracy) should be considered. As shown in Eq. (2), the sensors of the resultant sensor network configuration are deployed at the locations such that the configuration satisfies the required estimation accuracy with the longest operation lifetime. In the following section, we present the proposed cluster-based network optimization algorithm to configure the optimal wireless network with the longest lifespan based on the designated monitoring locations.

3. Cluster-based network optimization algorithm

In this section, we present the strategy to configure the optimal network $\mathbf{W_S^*}$ with the longest lifespan among all possible network configurations regarding the sensor locations $\mathbf{S}$. This approach consists of three phases which are network formation, network lifetime computation and network evaluation. In the first phase, all possible networks are formed through the cluster head selection, the cluster formation and the base station determination. In the second phase, the corresponding lifetime of each network is computed. Thereafter, in the third phase, all the possible networks are evaluated based on their lifetime to determine the optimal one. In the following, the formulation of the three phases is presented.

3.1 The first phase: *Network formation*

In this phase, the potential network configurations that satisfy the required identification accuracy are formed. In a wireless sensor network with multi-type sensors, each cluster contains only one type of sensors. Let N be the number of clusters in the network, where $N_{\mathcal{T}} \leq N \leq N_s$. First, all combinations with N cluster head nodes are formulated. For this purpose, N sensor nodes are selected randomly from $\mathbf{S}$ to be the cluster head nodes. The locations of the selected N cluster heads can be expressed as

$$\hat{\mathbf{C}}^{[N]} = \left\{ \hat{c}_{\tau,\eta}^{[N]} \middle| \tau = 1,2,\dots,N_{\mathcal{T}}; \eta = 1,2,\dots,N_{\hat{c}\tau}^{[N]} \right\} \tag{3}$$

where $\hat{c}_{\tau,\eta}^{[N]} \in \{s_{\tau,1}, s_{\tau,2}, \dots, s_{\tau,N_\tau}\}$ denotes the location of

the ηth cluster head node of the τth type sensor; the positive integer $N_{\hat{c}\tau}^{[N]}, \tau = 1,2,\dots,N_{\mathcal{T}}$, is the number of the τth type sensor in $\hat{\mathbf{C}}^{[N]}$ and it satisfies $\sum_{\tau=1}^{N_{\mathcal{T}}} N_{\hat{c}\tau}^{[N]} = N$. Hence, for a network with N cluster head nodes, the collection of the locations of the possible cluster head combinations are included in the set $\hat{\boldsymbol{\mathcal{C}}}^{[N]}$.

Next, we develop the clusters according to the cluster heads given by Eq. (3). Except the cluster head nodes $\hat{\mathbf{C}}^{[N]}$, the rest of the sensors in the sensor network are non-cluster head nodes and their locations are denoted as $\bar{\mathbf{C}}^{[N]}$, i.e., $\bar{\mathbf{C}}^{[N]} = \mathbf{S} - \hat{\mathbf{C}}^{[N]}$. Then, each non-cluster head node searches their nearest cluster head with the same sensor type. For the case that a non-cluster head node can has more than one choice, it selects the one that has the minimum number of corresponding non-cluster head nodes. For the cluster with cluster head at $\hat{c}_{\tau,\eta}^{[N]}$, the set of locations of all cluster members are

$$\mathbf{C}_{\tau,\eta}^{[N]} = \left\{\hat{c}_{\tau,\eta}^{[N]}\right\} \cup \left\{\bar{c}_{\tau,\eta,\mu}^{[N]} \middle| \mu = 1,2,\dots,N_{\bar{c}(\tau,\eta)}^{[N]}\right\}, \quad \tau = 1,2,\dots,N_{\mathcal{T}}, \eta = 1,2,\dots,N_{\hat{c}\tau}^{[N]} \tag{4}$$

where $\bar{c}_{\tau,\eta,\mu}^{[N]}$ denotes the location of the μth non-cluster head node with the closest cluster head node $\hat{c}_{\tau,\eta}^{[N]}$; $\left\{\bar{c}_{\tau,\eta,\mu}^{[N]} \middle| \mu = 1,2,\dots,N_{\bar{c}(\tau,\eta)}^{[N]}\right\}$ denotes the set that includes the locations of the non-cluster head nodes with the closest cluster head node $\hat{c}_{\tau,\eta}^{[N]}$; and $N_{\bar{c}(\tau,\eta)}^{[N]}$ is the number of the non-cluster head nodes in $\mathbf{C}_{\tau,\eta}^{[N]}$. To ensure the signal can be transmitted to the corresponding cluster head without information lost, the distance from all non-cluster head nodes in the cluster to the cluster head is within the transmission cluster radius ρ_c.

The next step is to determine the location of the base station given by $\hat{\mathbf{C}}^{[N]}$. The possible locations of the base station are indicated with $b_1, b_2, \dots, b_{N_b}$. For the β th location b_β, the sum of the distances between the base station to all cluster head nodes is denoted as

$$\mathbb{D}_\beta^{[N]} = \sum_{\tau=1}^{N_{\mathcal{T}}} \sum_{\eta=1}^{N_{\hat{c}\tau}^{[N]}} \left(d_{b,\beta,(\tau,\eta)}^{[N]}\right)^{\lambda_b} \tag{5}$$

where $d_{b,\beta,(\tau,\eta)}^{[N]}$ is the distance from the base station at b_β to the cluster head $\hat{c}_{\tau,\eta}^{[N]}$; and λ_b is the path loss exponent for transmitting data to the base station (Heinzelman *et al*. 2002). Therefore, the optimal location of the base station satisfies

$$b_{\beta^{*[N]}} = \underset{b_\beta}{\operatorname{argmin}}\, \mathbb{D}_\beta^{[N]} \tag{6}$$

where $\beta^{*[N]}$ is the index of the optimal location of the base station.

Based on the clusters obtained from Eq. (4) and the optimal location of the base station obtained from Eq. (6), the resultant wireless network configuration corresponding to $\hat{\mathbf{C}}^{[N]}$ is formulated as

$$\mathbf{W}_{\mathbf{S},\hat{\mathbf{C}}^{[N]}} = \left\{b_{\beta^{*[N]}}, \mathbf{C}_{\tau,\eta}^{[N]} \middle| \tau = 1,2,\dots,N_{\mathcal{T}}; \eta = 1,2,\dots,N_{\hat{c}\tau}^{[N]}\right\} \tag{7}$$

3.2 The second phase: Network lifetime computation

In this subsection, the lifetime of the formed wireless network $\mathbf{W}_{\mathbf{S},\hat{\mathbf{C}}^{[N]}}$ is computed. It indicates the energy dissipation of the battery-operated devices in the network. Based on Eq. (1), the lifetime depends on the rate of energy consumption of the dominated sensor node. In the following, we present the consumed energy of each non-cluster head node and cluster head node in the network. The dominated sensor node consumes the highest energy which is used to compute the lifetime of the network. In a wireless sensor network, the non-cluster head nodes transmit data to its cluster head. Then, the cluster head node performs data aggregation and transmits the aggregated data to the base station. A schematic plot of the energy consumption of a wireless sensor network configuration is shown in Fig. 1. Assume that there are N clusters in the network. In the figure, the square, circle with solid border and circle with dotted border represent the base station, cluster head node and non-cluster head node, respectively. The dotted arrow and solid arrow indicate the data transmission route from a non-cluster head node to a cluster head node and data transmission route from a cluster head to base station, respectively. For the cluster $\mathbf{C}_{\tau,\eta}^{[N]}$, it contains one cluster head node and $N_{\bar{c}(\tau,\eta)}^{[N]}\left(\mathbf{W}_{\mathbf{S},\hat{\mathbf{C}}^{[N]}}\right)$ non-cluster head nodes. Data is transmitted between wireless sensors by radio waves (Heinzelman *et al*. 2002). The energy consumption of the wireless network is the dissipated energy cumulated from all components in the network. In the following, the energy consumption of different components is presented.

For the non-cluster head node, energy is dissipated in the transmit mode, i.e., energy is used to transmit data from the non-cluster head node to the cluster head node. Regarding the cluster $\mathbf{C}_{\tau,\eta}^{[N]}$, the rate of energy consumption of the μth non-cluster head node is dissipated to transmit $l^{(\tau)}$ bits/s of data to the cluster head with distance $d_{\hat{c},\tau,\eta,\mu}^{[N]}(\mathbf{W}_{\mathbf{S},\hat{\mathbf{C}}^{[N]}})$ (Heinzelman *et al*. 2002)

$$E_{\bar{T}\mu}^{(\tau,\eta)}\left(\mathbf{W}_{\mathbf{S},\hat{\mathbf{C}}^{[N]}}\right) = \epsilon_T^{(\tau)} l^{(\tau)} + \alpha_{\bar{c}}^{(\tau)} l^{(\tau)} \left(d_{\hat{c},\tau,\eta,\mu}^{[N]}(\mathbf{W}_{\mathbf{S},\hat{\mathbf{C}}^{[N]}})\right)^{\lambda_{\hat{c}}} \tag{8}$$

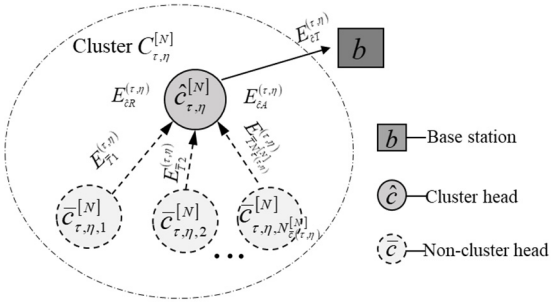

Fig. 1 Schematic plot of the energy consumption of the sensor nodes in wireless sensor network

where $\epsilon_T^{(\tau)}$ is the electronics energy coefficient for data transmission of the τth type sensor; $\alpha_{\hat{c}}^{(\tau)}$ is the transmitter power amplifier cost coefficient of the non-cluster head node of the τth type; and $\lambda_{\hat{c}}$ is the path loss exponent for transmitting data to the cluster head node.

For the cluster head node, the energy is consumed to receive data from the non-cluster head nodes, aggregate data, and transmit aggregate data to the base station. Regarding the cluster head node of the cluster $\mathbf{C}_{\tau,\eta}^{[N]}$, the rate of energy consumption of receiving data from the non-cluster head nodes is (Heinzelman *et al*. 2002)

$$E_{\hat{c}R}^{(\tau,\eta)}\left(\mathbf{W}_{\mathbf{S},\hat{\mathbf{C}}^{[N]}}\right) = \epsilon_R^{(\tau)} l^{(\tau)} N_{\tilde{c}(\tau,\eta)}^{[N]}\left(\mathbf{W}_{\mathbf{S},\hat{\mathbf{C}}^{[N]}}\right) \tag{9}$$

where $\epsilon_R^{(\tau)}$ is the electronics energy coefficient for data reception of the τth type sensor. The rate of energy consumption of aggregating data at the cluster head node of the cluster $\mathbf{C}_{\tau,\eta}^{[N]}$ is (Heinzelman *et al*. 2002)

$$E_{\hat{c}A}^{(\tau,\eta)}\left(\mathbf{W}_{\mathbf{S},\hat{\mathbf{C}}^{[N]}}\right) = \epsilon_A^{(\tau)} l^{(\tau)}\left(N_{\tilde{c}(\tau,\eta)}^{[N]}\left(\mathbf{W}_{\mathbf{S},\hat{\mathbf{C}}^{[N]}}\right) + 1\right) \tag{10}$$

where $\epsilon_A^{(\tau)}$ is the energy coefficient for data aggregation of the τth type sensor. The rate of energy consumption of transmitting data from the cluster head in $\mathbf{C}_{\tau,\eta}^{[N]}$ to the base station with distance $d_{b,(\tau,\eta)}^{[N]}(\mathbf{W}_{\mathbf{S},\hat{\mathbf{C}}^{[N]}})$ is

$$\begin{aligned} &E_{\hat{c}T}^{(\tau,\eta)}\left(\mathbf{W}_{\mathbf{S},\hat{\mathbf{C}}^{[N]}}\right) \\ &= \epsilon_T^{(\tau)} l^{(\tau)} + \alpha_{\hat{c}}^{(\tau)} l^{(\tau)}\left(d_{b,(\tau,\eta)}^{[N]}\left(\mathbf{W}_{\mathbf{S},\hat{\mathbf{C}}^{[N]}}\right)\right)^{\lambda_b} \end{aligned} \tag{11}$$

where $\alpha_{\hat{c}}^{(\tau)}$ is the transmitter power amplifier cost coefficient of the cluster head node of the τth type; λ_b is the path loss exponent for transmitting data to the base station.

Therefore, the total rate of energy consumption of the cluster head node in $\mathbf{C}_{\tau,\eta}^{[N]}$ is

$$\begin{aligned} E_{\hat{c}}^{(\tau,\eta)}\left(\mathbf{W}_{\mathbf{S},\hat{\mathbf{C}}^{[N]}}\right) = E_{\hat{c}R}^{(\tau,\eta)}\left(\mathbf{W}_{\mathbf{S},\hat{\mathbf{C}}^{[N]}}\right) + E_{\hat{c}A}^{(\tau,\eta)}\left(\mathbf{W}_{\mathbf{S},\hat{\mathbf{C}}^{[N]}}\right) \\ + E_{\hat{c}T}^{(\tau,\eta)}\left(\mathbf{W}_{\mathbf{S},\hat{\mathbf{C}}^{[N]}}\right) \end{aligned} \tag{12}$$

Based on Eqs. (8) and (12), the rate of energy consumption of each non-cluster head node and cluster head node can be computed. Consequently, the maximum rate of energy consumption of all these sensor nodes in the network $\mathbf{W}_{\mathbf{S},\hat{\mathbf{C}}^{[N]}}$ is

$$\begin{aligned} &E_{\mathcal{M}}\left(\mathbf{W}_{\mathbf{S},\hat{\mathbf{C}}^{[N]}}\right) \\ &= \max_{\substack{\tau=1,\dots,N_{\mathcal{T}},\\ \eta=1,\dots,N_{\hat{c}\tau}^{[N]},\\ \mu=1,\dots,N_{\tilde{c}(\tau,\eta)}^{[N]}}} \left\{E_{\hat{c}}^{(\tau,\eta)}\left(\mathbf{W}_{\mathbf{S},\hat{\mathbf{C}}^{[N]}}\right), E_{\bar{\tau}\mu}^{(\tau,\eta)}\left(\mathbf{W}_{\mathbf{S},\hat{\mathbf{C}}^{[N]}}\right)\right\} \end{aligned} \tag{13}$$

Finally, Eq. (1) can be rewritten to represent the lifetime of the network $\mathbf{W}_{\mathbf{S},\hat{\mathbf{C}}^{[N]}}$

$$L\left(\mathbf{W}_{\mathbf{S},\hat{\mathbf{C}}^{[N]}}\right) = \frac{\varepsilon_0}{E_{\mathcal{M}}\left(\mathbf{W}_{\mathbf{S},\hat{\mathbf{C}}^{[N]}}\right)} \tag{14}$$

where ε_0 is the stored energy of each sensor node. A larger value implies that the network can fully operate for a longer time.

3.3 The third phase: Network evaluation

In the third phase, the performance of all potential network configurations are compared. The optimal one is formulated based on the sensors with location $\mathbf{S}$ and can be operated with the longest lifespan.

Based on the first phase, the wireless networks with N clusters corresponding to all possible cluster head combinations in $\widehat{\mathcal{C}}^{[N]}$ can be obtained. and the collection of all possible clusters is denoted as

$$\mathcal{W}^{[N]} = \left\{\mathbf{W}_{\mathbf{S},\hat{\mathbf{C}}^{[N]}} : \hat{\mathbf{C}}^{[N]} \in \widehat{\mathcal{C}}^{[N]}\right\} \tag{15}$$

By changing the number of clusters N from $N_{\mathcal{T}}$ to N_s, all possible network configurations of $\mathbf{S}$ can be obtained. In the second phase, the lifetime of these network configurations are computed based on Eq. (14). Finally, the optimal cluster-based network $\mathbf{W}_{\mathbf{S}}^*$ of $\mathbf{S}$ is obtained as the one that maximizes the lifetime

$$L(\mathbf{W}_{\mathbf{S}}^*) = \max_{\substack{N_{\mathcal{T}} \le N \le N_s \\ \hat{\mathbf{C}}^{[N]} \in \widehat{\mathcal{C}}^{[N]}}} \left\{L\left(\mathbf{W}_{\mathbf{S},\hat{\mathbf{C}}^{[N]}}\right)\right\} \tag{16}$$

In the next section, we present the formulation for structural identification to quantify the uncertainty in the estimated parameters. It will be used to evaluate the quality of information captured by different wireless sensor network configurations.

4. Structural identification

The Bayesian spectral density approach (Katafygiotis and Yuen 2001) is utilized for structural identification. It is a Bayesian based frequency-domain approach that uses the statistic properties of the spectral density estimator to obtain the optimal model parameters and their associated estimation uncertainty. During the design stage of sensor network configuration, structural response measurement is not yet available and the properties of the structural nominal model are utilized to proceed the design. The equation of motion for the concerned N_d DOFs structure can be expressed as

$$\mathbf{M}(\boldsymbol{\vartheta}_M)\ddot{\mathbf{x}}(t) + \mathbf{D}(\boldsymbol{\vartheta}_M)\dot{\mathbf{x}}(t) + \mathbf{K}(\boldsymbol{\vartheta}_M)\mathbf{x}(t) = \mathbf{V}\mathbf{f}(t) \tag{17}$$

where $\mathbf{x}(t)$ is the generalized displacement vector of the structure at time t; $\mathbf{M}(\boldsymbol{\vartheta}_M) \in \mathbb{R}^{N_d \times N_d}$, $\mathbf{D}(\boldsymbol{\vartheta}_M) \in \mathbb{R}^{N_d \times N_d}$ and $\mathbf{K}(\boldsymbol{\vartheta}_M) \in \mathbb{R}^{N_d \times N_d}$ are the mass, damping and stiffness matrix of the structure, respectively; $\boldsymbol{\vartheta}_M$ is the structural model parameter vector that parameterize with the mass, damping and stiffness matrix; $\mathbf{f}(t) \in \mathbb{R}^{N_f}$ is the excitation that parameterized with the excitation parameter vector $\boldsymbol{\vartheta}_f$;

$\mathbf{V} \in \mathbb{R}^{N_d \times N_f}$ is the excitation distributing matrix. The instrumented response vector $\mathbf{z}(t) \in \mathbb{R}^{N_z}$ contains all possible quantities to be measured based on the available type of sensors and it is given by

$$\mathbf{z}(t) = \mathbf{T}[\mathbf{x}(t)^T, \dot{\mathbf{x}}(t)^T, \ddot{\mathbf{x}}(t)^T]^T \tag{18}$$

where $\mathbf{T} \in \mathbb{R}^{N_z \times 3N_d}$ is the transformation matrix that maps the extended system state $[\mathbf{x}(t)^T, \dot{\mathbf{x}}(t)^T, \ddot{\mathbf{x}}(t)^T]^T$ to $\mathbf{z}(t)$. Then, at mth time step, $m = 1,2, \ldots$, the observed data $\mathbf{y}_\mathbf{S}(m) \in \mathbb{R}^{N_s}$ is given by

$$\mathbf{y}_\mathbf{S}(m) = \mathbf{G}(\mathbf{S})\mathbf{z}(m) + \boldsymbol{\varepsilon}_\mathbf{S}(m) \tag{19}$$

where $\mathbf{z}(m)$ is the quantity to be measured at time $t_m = m\Delta t$; Δt is the sampling time interval; and $\boldsymbol{\varepsilon}_\mathbf{S}(m)$ is the modeling error. The modeling error is taken as a zero-mean Gaussian process with covariance matrix governed by the prediction-error parameter vector $\boldsymbol{\vartheta}_\varepsilon$.

The collection of measurements of the first N_t time steps $\mathbf{Y}_\mathbf{S} = \{\mathbf{y}_\mathbf{S}(m), m = 1,2, \ldots, N_t\}$ can be used to update the probability distribution of the parameter vector $\boldsymbol{\vartheta} = [\boldsymbol{\vartheta}_M^T, \boldsymbol{\vartheta}_f^T, \boldsymbol{\vartheta}_\varepsilon^T]^T \in \mathbb{R}^{N_\vartheta}$. A discrete estimator of the power spectral density matrix is expressed as

$$\boldsymbol{\mathcal{P}}_\mathbf{S}(\omega_l) = \frac{\Delta t}{2\pi N_t} \sum_{m,m'=0}^{N_t-1} \mathbf{y}_\mathbf{S}(m)\, \mathbf{y}_\mathbf{S}(m')^* \exp[-i\omega_l(m - m')\Delta t] \tag{20}$$

where $\omega_l = l\Delta\omega, l = 0,1, \ldots, \mathrm{INT}(N_t/2)$, $\Delta\omega = 2\pi/N_t\Delta t$. The superscript * denotes the conjugate transpose of a vector. Given N_ρ independent sets of measured data, one can compute the corresponding discrete estimator of the power spectral density matrix $\boldsymbol{\mathcal{P}}_\mathbf{S}^{(\rho)}(\omega_l)$, $\rho = 1, \ldots, N_\rho$ using Eq. (20). Then, the averaged spectral density matrix estimator can be obtained

$$\boldsymbol{\mathcal{P}}_\mathbf{S}^{avg}(\omega_l) = \frac{1}{N_\rho} \sum_{\rho=1}^{N_\rho} \boldsymbol{\mathcal{P}}_\mathbf{S}^{(\rho)}(\omega_l) \tag{21}$$

By using the Bayes' theorem, the updated probability density function (PDF) of the uncertain parameter vector is given by (Katafygiotis and Yuen 2001)

$$p(\boldsymbol{\vartheta}|\mathbf{Y}_\mathbf{S}) = \kappa_0 p(\boldsymbol{\vartheta}) p(\mathbf{Y}_\mathbf{S}|\boldsymbol{\vartheta}) \tag{22}$$

where κ_0 is the normalizing constant; $p(\boldsymbol{\vartheta})$ is the prior PDF; and $p(\mathbf{Y}_\mathbf{S}|\boldsymbol{\vartheta})$ is the likelihood function that reflects the contribution of measurement $\mathbf{Y}_\mathbf{S}$ in establishing the updated PDF of $\boldsymbol{\vartheta}$.

Based on the Bayesian spectral density approach (Katafygiotis and Yuen 2001), the likelihood function is

$$p(\mathbf{Y}_\mathbf{S}|\boldsymbol{\vartheta}) = \kappa_1 \prod_{\omega_l \in \Xi} \frac{1}{|E[\boldsymbol{\mathcal{P}}_\mathbf{S}(\omega_l)|\boldsymbol{\vartheta}]|^{N_\rho}} \exp(-N_\rho tr\{E[\boldsymbol{\mathcal{P}}_\mathbf{S}(\omega_l)|\boldsymbol{\vartheta}]^{-1} \boldsymbol{\mathcal{P}}_\mathbf{S}^{avg}(\omega_l)\}) \tag{23}$$

where κ_1 is the normalizing constant; $E[.|\boldsymbol{\theta}]$ denoting the mathematical expectation; $tr(\cdot)$ and $|\cdot|$ are the trace and determinant of a matrix, respectively. Hence, the updated PDF in Eq. (22) can be obtained. Then, the objective function can be defined as the negative logarithm of the updated PDF

$$J(\boldsymbol{\vartheta}) = -\ln[p(\boldsymbol{\vartheta}|\mathbf{Y}_\mathbf{S})] \tag{24}$$

The optimal parameters $\boldsymbol{\vartheta}_\mathbf{S}^*$ can be obtained by the minimizing $J(\boldsymbol{\vartheta})$. Furthermore, the updated PDF can be approximated by a Gaussian distribution $\mathcal{G}(\boldsymbol{\vartheta}_\mathbf{S}^*, \sum_\mathbf{S})$, where the covariance matrix $\sum_\mathbf{S}$ is equal to the inverse of the Hessian $\mathbf{Q}(\boldsymbol{\vartheta}_\mathbf{S}^*, \mathbf{Y}_\mathbf{S})$ of the objective function calculated at $\boldsymbol{\vartheta} = \boldsymbol{\vartheta}_\mathbf{S}^*$. Thereafter, the COV of the ith estimated parameter is the square root of the (i,i)th component of $\sum_\mathbf{S}$ divided by the ith optimal parameter $\boldsymbol{\vartheta}_\mathbf{S}^{*(i)}$

$$\xi_\mathbf{S}^{(i)} = \sqrt{\boldsymbol{\Sigma}_\mathbf{S}^{(i,i)}} / \boldsymbol{\vartheta}_\mathbf{S}^{*(i)}, \quad i = 1, 2, \ldots, N_\vartheta \tag{25}$$

Hence, the COV of all N_ϑ estimated parameters can be obtained. Finally, the maximum COV value is utilized as the indicator of estimation accuracy

$$\xi_{\mathbf{S},\mathcal{M}} = \max_{i=1,2,\ldots,N_\vartheta} \left(\sqrt{\boldsymbol{\Sigma}_\mathbf{S}^{(i,i)}} / \boldsymbol{\vartheta}_\mathbf{S}^{*(i)} \right) \tag{26}$$

where N_ϑ is the number of the uncertain parameters. For more details, please refer to Katafygiotis and Yuen (2001). Based on the COV, estimation accuracy achieved by the sensors with $\mathbf{S}$ can be evaluated. It provides a holistic measure to evaluate the quality of information captured by a wireless sensor network regardless the sensor type and network configuration. This is important for the quality assurance of the system identification results for post-processing (Yuen and Katafygiotis 2005, Yuen *et al*. 2007). If the resultant COV of the estimated parameters do not fulfill the requirement, the underlying wireless sensor network configuration will not be employed.

Based on the lifetime obtained from Eq. (16) and the resultant maximum COV of the parameters obtained from Eq. (26), the performance of the sensors with $\mathbf{S}$ can be evaluated. Due to the large number of the possible sensor network configurations, it is expensive to evaluate the performance of all the possible configurations. Genetic algorithm (GA) is implemented to find the optimal solution for this sensor placement optimization problem as it is an effective algorithm that based on highly parallel blind search. GA (Yi and Li 2012, Liu *et al*. 2008, Liu *et al*. 2015) evolves in an analogous manner as the natural evolution of a species. The main procedure is given as follows. First, N_p initial populations that represent N_p different N_s-sensor configurations are generated. The collection of the generated configurations of the gth generation is denoted as $\boldsymbol{\mathcal{S}}_g = \{\mathbf{S}_{g,1}, \mathbf{S}_{g,2}, \ldots, \mathbf{S}_{g,N_p}\}$. The initial generation starts with $g = 0$. Then, the function optimization criteria given by Eq. (2) are established to evaluate the performance of each candidate. Bayesian inference is implemented to

quantify the uncertainty of the estimated parameters. The estimation accuracy of $\mathbf{S}_{g,q}, q = 1,2,\dots,N_p$ is evaluated based on the maximum COV of the estimated parameters $\xi_{\mathbf{S}_{g,q},\mathcal{M}}$. Finally, the initial population undergoes generational evolution (natural selection, crossover and mutation) until the absolute percentage change in the lifetime is less than the acceptable tolerance (e.g., 0.01%). The one with the maximum lifetime will be selected as the optimal design.

5. Summary

The procedure of the proposed method is summarized in the following:

1. Initial generation ($g = 0$):
   Generate the initial populations randomly.
2. Establish the set $\boldsymbol{S}_g = \left\{\mathbf{S}_{g,1}, \mathbf{S}_{g,2}, \dots, \mathbf{S}_{g,N_p}\right\}$ to include all the generated sensor configurations and evaluate the performance of each configuration:
   <1> Let $q = 1$.
   <2> Compute $\xi_{\mathbf{S}_{g,q},\mathcal{M}}$ using Eq. (26) and compare it with the required COV threshold ξ_r.
   If $\xi_{\mathbf{S}_{g,q},\mathcal{M}} < \xi_r$, go to Step <3>; otherwise, remove $\mathbf{S}_{g,q}$. Then, increase q by 1 and repeat from Step <2> until $\xi_{\mathbf{S}_{g,q},\mathcal{M}} < \xi_r$.
   <3> Determine the optimal clustering network for $\mathbf{S}_{g,q}$.
   The first phase (network formation):
   i. Let $N = N_{\mathcal{T}}$.
   ii. Cluster head selection: formulate $\hat{\mathbf{C}}^{[N]}$ using Eq. (3) and obtain $\hat{\boldsymbol{C}}^{[N]}$.
   iii. Cluster formation: form $\mathbf{C}_{\tau,\eta}^{[N]}$, $\tau = 1,\dots,N_{\mathcal{T}}, \eta = 1,\dots,N_{\hat{c}\tau}^{[N]}$ using Eq. (4).
   iv. Base station determination: select $b_{\beta^{*[N]}}$ using Eq. (6).
   v. Network formation: form $\mathbf{W}_{\mathbf{S}_{g,q},\hat{\mathbf{C}}^{[N]}}$ using Eq. (7).
   vi. Form $\boldsymbol{\mathcal{W}}^{(N)}$ using Eq. (15).
   If $N < N_s$, increase N by 1 and repeat the procedure from Step ii; otherwise go to Step vii.
   vii. Obtain all possible networks for $\mathbf{S}_{g,q}$.
   The second phase (network lifetime computation):
   viii. Calculate the lifetime for each network using Eq. (14).
   The third phase (network evaluation):
   ix. Determine the optimal network $\mathbf{W}_{\mathbf{S}_{g,q}}^{*}$.
   <4> Obtain the lifetime $L\left(\mathbf{W}_{\mathbf{S}_{g,q}}^{*}\right)$ using Eq. (16).
   If $q < N_p$, increase q by 1 and repeat the procedure from Step <2>; otherwise, go to Step <5>.
   <5> Evaluate the lifetime of each configuration in $\boldsymbol{S}_g$.
   If the change of the lifetime is not less than the acceptable tolerance, perform the evolution of populations (natural selection, crossover and mutation). Increase g by 1 and repeat from Step 2; otherwise, go to Step 3.
3. Obtain the optimal design with the longest lifespan using Eq. (2).

6. Illustrative examples

To demonstrate the performance of the proposed method, two examples are presented. In particular, the first example considers the optimal wireless sensor network configuration of Ting Kau Bridge model under various conditions. The second example considers the versatile wireless sensor network design of a space truss.

6.1 Example 1: Ting Kau Bridge model

In this example, the proposed method is applied to design the optimal information and lifespan wireless sensor network of the Ting Kau bridge (shown in Fig. 2). It is a cable-stayed bridge with three towers. The bridge has two main spans with 448 m and 475 m and two side spans with equal length of 127 m. There are two carriageways with width of 18.8 m each in the bridge deck. Detailed information of the Ting Kau bridge benchmark structural health monitoring can be found in Wong (2004), Ni *et al*. (2015) and Kuok and Yuen (2016). In this study, the bridge is modeled as a structure with 37 nodes and 36 members. Its finite element model is shown in Fig. 3. The bolded numbers and the numbers in parenthesis denote the node numbers and the numbering for the members, respectively. Based on the finite element model of the bridge, the first five nominal natural frequencies are 0.146 Hz, 0.194 Hz, 0.214 Hz, 0.292 Hz and 0.349 Hz. Rayleigh damping model is considered, i.e., $\mathbf{D} = \varphi_{\mathrm{M}}\mathbf{M} + \varphi_{\mathrm{K}}\mathbf{K}$, where φ_{M} and φ_{K} are $1.045 \times 10^{-2}\ \mathrm{s}^{-1}$ and $9.378 \times 10^{-3}\ \mathrm{s}$, respectively. As a result, the damping ratios of the first two modes are 1%. The bridge was subjected to horizontal and vertical excitations, which were modeled as zero-mean Gaussian white noise with a spectral intensity $5 \times 10^{-4}\ \mathrm{m}^2/\mathrm{s}^3$. The measured response is assumed to consist of horizontal acceleration and vertical acceleration. The stiffness matrix $\mathbf{K}$ is parameterized with eleven parameters. Specifically, ϑ_{k1}, ϑ_{k2}, ϑ_{k3}, ϑ_{k4}, ϑ_{k5}, ϑ_{k6}, ϑ_{k7} and ϑ_{k8} were assigned to the 1st-2nd, 3rd-5th, 6th-8th, 9th-11th, 12th-14th, 15th-17th, 18th-21th and 22th-23th deck members, respectively; ϑ_{k9}, ϑ_{k10}, and ϑ_{k11} were assigned to the 24th-27th, 28th-32th and 33th-36th tower members, respectively. Accelerometers with sampling rate 200 Hz were installed for the identification of the uncertain stiffness parameters. Assume that the stored energy ε_0 of each sensor node is $1 \times 10^5\ \mathrm{J}$. The communication energy parameters of wireless sensors are set as (Heinzelman *et al*. 2002): $\epsilon_T = 45\ \mathrm{nJ/bit}$, $\epsilon_R = 135\ \mathrm{nJ/bit}$, $\alpha_{\bar{c}} = 10\ \mathrm{pJ/bit/m^2}$, $\alpha_{\hat{c}} = 0.0013\ \mathrm{pJ/bit/m^4}$, $\epsilon_A = 5\ \mathrm{nJ/bit/signal}$, $\lambda_{\hat{c}} = 2$, $\lambda_b = 4$, $\rho_c = 200\ \mathrm{m}$, and $l = 4800\ \mathrm{bit/s}$.

6.1.1 Effectiveness of the network optimization

First, we evaluate the performance of the proposed optimal wireless network configuration approach. Ten locations are randomly selected from the structure for wireless accelerometers, i.e., the y-direction of the 2nd, the

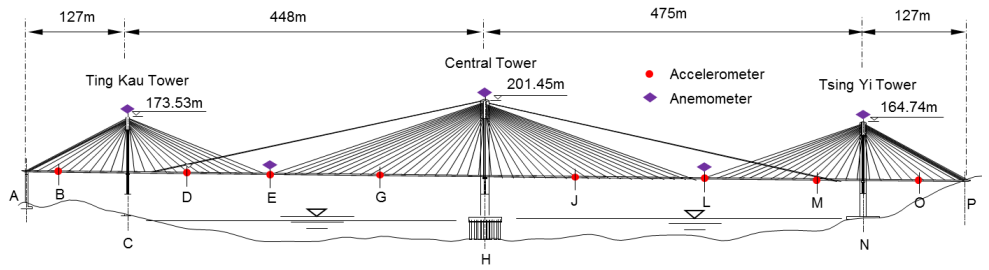

Fig. 2 Ting Kau Bridge (TKB) (provided by Ni *et al*. 2015)

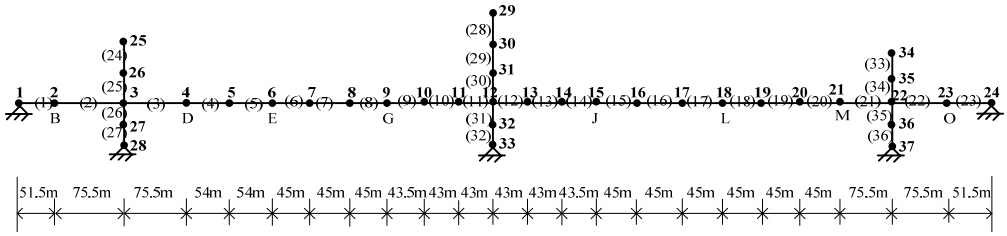

Fig. 3 Bridge model

5th, the 7th, the 13th, the 20th, and the 21st node and the x-direction of the 27th, the 29th, the 31st and the 36th node. The optimal network obtained by the proposed cluster-based network optimization algorithm is shown in Fig. 4. The non-cluster head node, cluster head node, base station are indicated by a circular marker with dotted border, a circular marker with solid border and a square marker, respectively. The arrows inside the cluster/non-cluster head nodes indicates the monitoring directions. The data transmission route from the non-cluster head node to the cluster head node and the data transmission route from the cluster head node to the base station are indicated by a dotted arrow and a solid arrow, respectively.

The result shows that the optimal number of the clusters is four. The optimal cluster head nodes are placed at the y-direction of the 7th and the 20th node and the x-direction of the 27th and the 31st node. The base station is located at the 11th structural node. The resultant rate of energy consumption of each sensor in the optimal network configuration is shown in Table 1 with the cluster head nodes and their results in bold. It is observed that the rate of energy consumption of the cluster head nodes is larger than that of the non-cluster head nodes. The cluster head node at the x-direction of the 27th structural node consumes the highest energy ($0.1713\,\mathrm{J/s} = 616.68\,\mathrm{J/h}$). Hence, this node is the dominated node of the network and the lifetime of the optimal network configuration is 162 h. It indicates that this optimal network will be out of battery if no recharging is available.

For comparison, additional deployment scheme is investigated. The sensors remain at the ten locations as mentioned above. A flat network with the base station fixed in the center of the structure (i.e., the 12th structural node) is formed. Hence, the network forms a single-hop communication so each sensor node transmits data directly to the base station. The resultant rate of energy consumption of each sensor node in the flat network configuration is shown in Table 2. It is observed that the sensor node at the y-direction of the 2nd node consumes the most energy. As a result, the lifetime of the flat network configuration is 59 h, which is only 36% of the proposed method. Furthermore, the total rate of energy consumption of the flat network configuration (4985.64 J/h) is 4.9 times of that of the network configuration obtained by the proposed method (1026.25 J/h). It clearly indicates that the optimal network configuration obtained by the proposed cluster-based network optimization algorithm has higher energy efficiency and a longer lifespan.

6.1.2 Overall results

In this subsection, the optimal configurations with different number of accelerometers are demonstrated. Comparison between the optimal network configuration obtained by the proposed method and the network

Table 1 Rate of energy consumption of each sensor node in the cluster-based network

Sensor node (No. of node-direction)	2-y	5-y	**7-y**	13-y	**20-y**
E (J/h)	1.97	2.47	**25.2**	0.78	**366.64**
Sensor node (No. of node-direction)	21-y	**27-x**	29-x	**31-x**	36-x
E (J/h)	0.77	**616.68**	2.13	**6.12**	3.49

Table 2 Rate of energy consumption of each sensor node in the flat network

Sensor node (No. of node-direction)	2-y	5-y	7-y	13-y	20-y
E (J/h)	1688.04	232.2	52.92	1.08	355.68
Sensor node (No. of node-direction)	21-y	27-x	29-x	31-x	36-x
E (J/h)	573.12	916.92	7.56	1.08	1157.04

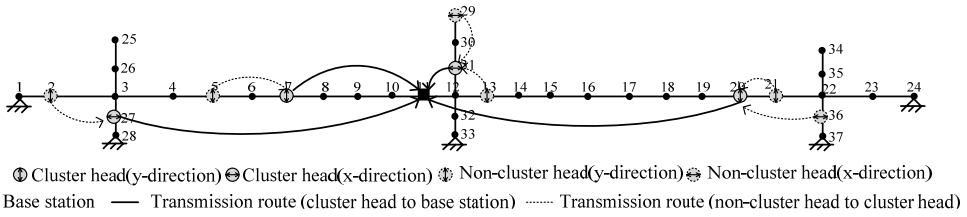

Fig. 4 Network configuration of the proposed method

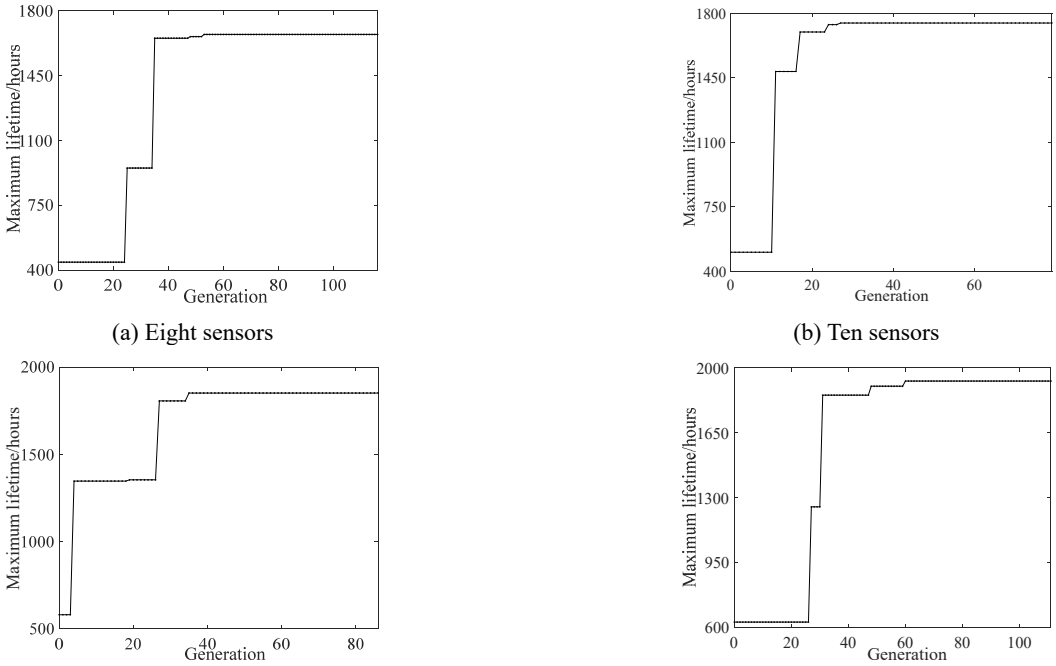

(a) Eight sensors

(b) Ten sensors

(c) Twelve sensors

(d) Fourteen sensors

Fig. 5 Convergence process of the objective function with (a) eight; (b) ten; (c) twelve; and (d) fourteen sensors

configurations with the sensors uniformly distributed over the structure is carried out. Regarding the uniformly distributed sensors, eight sensors are placed on the 2nd, 4th, 6th, 9th, 15th, 18th, 21st and 23rd node of the deck, which have the same as in-plane coordinates as the in-field monitoring. The other sensors are placed on the towers and/or the piers.

The required maximum COV threshold of the estimated stiffness parameters is 1.0%. The optimal solution is resolved based on the GA optimization. The population size is 50, the probability of crossover and the probability of mutation are set as the commonly used values of 0.8 and 0.05, respectively (Fang *et al*. 2018). Fig. 5 shows the convergence process of the objective function for the networks with eight, ten, twelve and fourteen sensors. It is observed that the maximum lifetime increases significantly at the early generation stage. As the number of generations increases, the maximum lifetime value tends to a constant.

In the same fashion as Fig. 4, Fig. 6 shows the optimal configurations with eight, ten, twelve and fourteen sensors. The resultant number of clusters in these four optimal configurations is four. It is found that the nodal response of the y-direction of the 6th, 13th and 15th node, and the x-direction of the 26th and 30th node (i.e., 6-y, 13-y, 15-y, 26-x and 30-x) are critical. These five nodal responses are common monitoring locations in all the four optimal configurations. Furthermore, in all the four optimal configurations, the sensors at the y-direction of the 6th and 15th node are the farthest cluster head nodes on both sides of the base station.

For comparison, we conducted the same analysis for the configurations with eight, ten, twelve and fourteen sensors that are uniformly distributed over the structure. The sensor patterns are {2-y, 4-y, 6-y, 9-y, 15-y, 18-y, 21-y, 23-y}, {2-y, 4-y, 6-y, 9-y, 15-y, 18-y, 21-y, 23-y, 26-x, 35-x}, {2-y, 4-y, 6-y, 9-y, 15-y, 18-y, 21-y, 23-y, 26-x, 30-x, 32-x, 35-x} and {2-y, 4-y, 6-y, 9-y, 15-y, 18-y, 21-y, 23-y, 26-x, 27-x, 30-x, 32-x, 35-x, 36-x}. The formation wireless networks are obtained based on the proposed cluster-based network optimization algorithm and their results are shown in Fig. 7. The number of clusters of the networks with eight and ten sensors is four while that of the network with twelve and fourteen sensors are five.

The resultant COV of the eleven estimated stiffness parameters of the concerned configurations are shown in Fig. 8. It summarizes the results of the configurations with eight, ten, twelve and fourteen sensors. As expected, for both optimal configuration and configuration with uniformly distributed sensors, the resultant COV of estimated parameters of the configuration with eight sensors

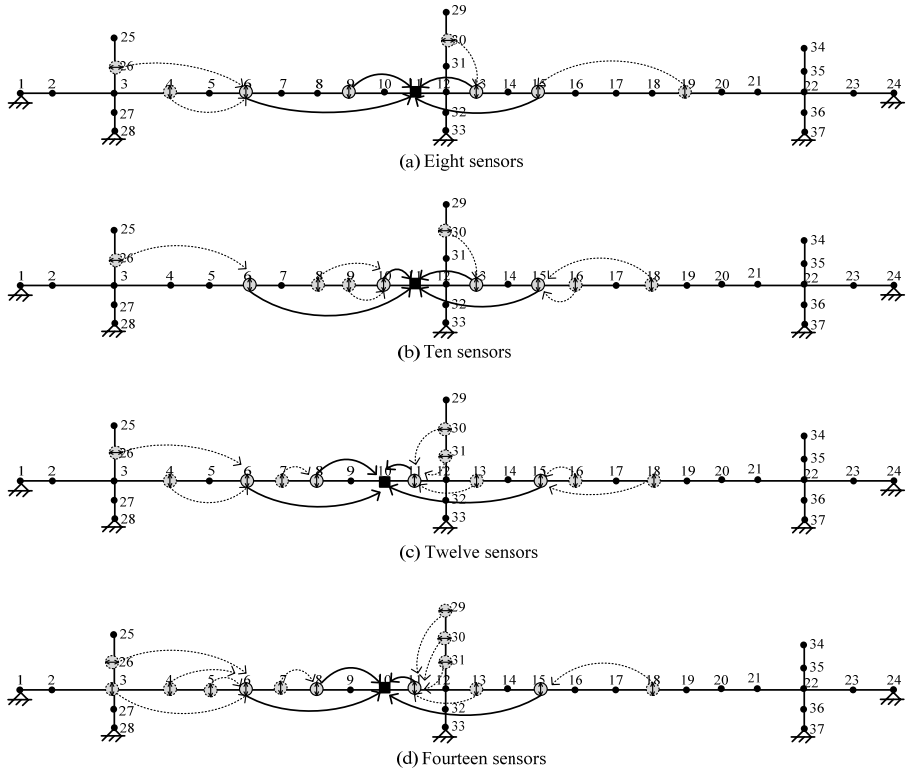

Fig. 6 Optimal sensor configurations with eight, ten, twelve and fourteen sensors

are generally higher than that of the configurations with more sensors. It indicates that the estimation accuracy of the less available sensors is the lowest. For the optimal configuration, the maximum COV of the parameters decreases as additional sensors are introduced. For the optimal configuration with eight, ten, twelve and fourteen sensors, the maximum COV occurred at ϑ_{k8} with 0.90%, 0.84%, 0.80% and 0.79%, respectively. The maximum COV of the parameters of the uniform eight-sensor configuration is as high as 1.46%. Furthermore, except the uniform eight-sensor configuration, the maximum COV of the parameters of the other three uniform sensor configurations do not exceed 0.6%.

Table 3 shows the network rate of energy consumption, dominated node, dominated node rate of energy consumption and lifetime for the optimal and uniform configurations with eight, ten, twelve and fourteen sensors. The third column shows the network rate of energy consumption of the sensor configurations. The fourth and the fifth column indicate the dominated node of the configuration and the corresponding rate of energy consumption, respectively. The sixth column shows the resultant lifetime of the sensor configurations. It is observed that for the optimal sensor configuration, the network rate of energy consumption increases as the number of sensors increases. The network rate of energy consumption of the optimal fourteen-sensor configuration is 133.2 J/h, which is1.2 times of that of the optimal eight-sensor configuration. On the other hand, the dominated sensor node of the optimal configurations with eight and ten sensors is at the y-direction of the 6th structural node, while the dominated node of the optimal configurations with twelve and fourteen sensors is at the y-direction of the 15th node. According to the resultant optimal configurations, the rate of energy consumption of the dominated nodes decreases when additional sensors are introduced. When the number of sensors of the optimal design increases, more sensors are placed near the base station. It turns out that the data transmission distance of the cluster heads to the base station is shortened. Therefore, the energy consumed by the dominated node is reduced. Consequently, the corresponding lifetime of the optimal configuration

Table 3 Network rate of energy consumption, dominated node, dominated node rate of energy consumption and lifetime

	No. of sensors	E_{total} (J/h)	Dominated node	$E_{\mathcal{M}}$ (J/h)	L (h)
Optimal configuration	8	108.01	6-y	59.76	1673
	10	110.88	6-y	57.24	1747
	12	117.36	15-y	54.01	1852
	14	133.20	15-y	51.84	1929
Uniform configuration	8	1046.52	21-y	575.64	174
	10	1055.88	21-y	577.80	173
	12	1058.04	21-y	577.80	173
	14	1066.68	21-y	580.32	172

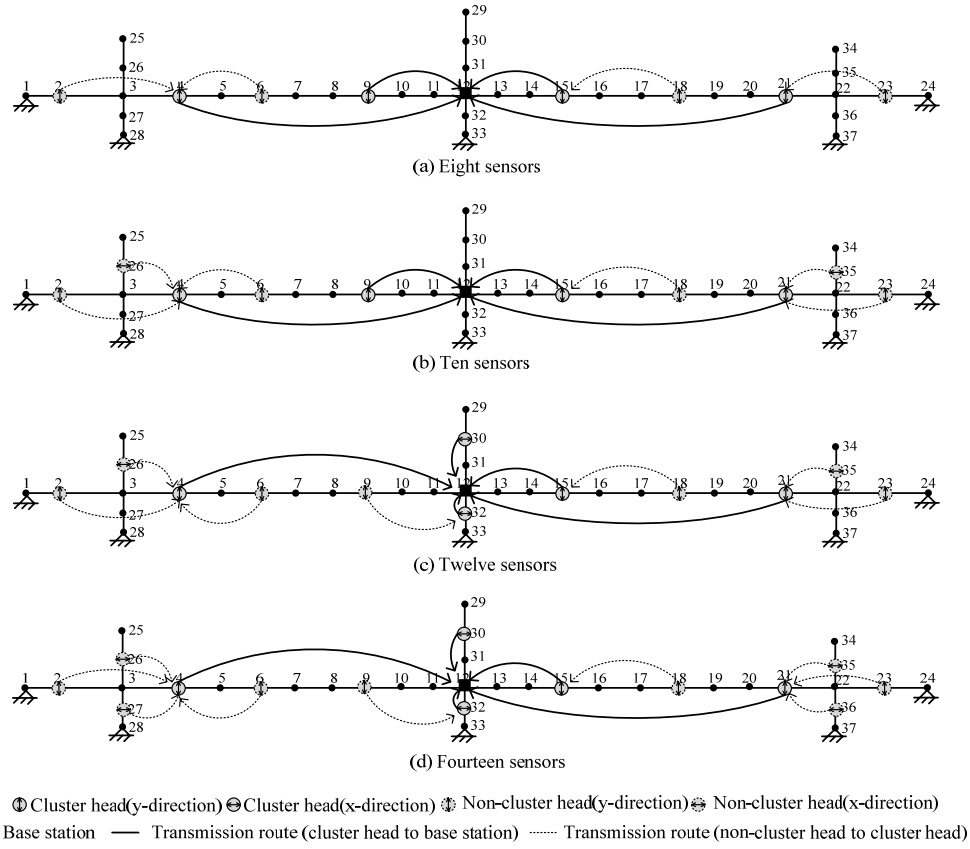

Fig. 7 Uniform sensor configurations with eight, ten, twelve and fourteen sensors

increases. The lifetime of the optimal fourteen-sensor configuration is 1929 h which is longer than that of the optimal configuration of eight sensors. For the four uniform sensor configurations, the dominated node in the network is the cluster head at the 21st node which has the farthest distance to the base station.

By comparing the optimal configuration and uniform configuration, it is found that the network rate of energy consumption of the optimal sensor configuration is smaller than that of the uniform sensor configuration when the number of sensors is fixed. Besides, the rate of energy consumption of the dominated node of the optimal configuration is smaller than that of the uniform configuration with the same number of sensors. With the optimized arrangement, the optimal sensor configuration has a longer lifespan than the uniform configuration with the same number of sensors. For example, for eight sensors, the lifetime of the optimal configuration by the proposed method is 1673 h and it is 9.6 times longer than that of the configuration with uniformly distributed sensors. The result confirms that the optimal design by the proposed method achieves satisfactory performance on maximizing the lifespan of a wireless network.

If the dominated sensor node in the optimal sensor configuration runs out of the battery, the corresponding COV of the estimated parameters will increase. Taking the optimal eight-sensor configuration as an example, the energy exhaustion of the dominated sensor node that located at the y-direction of the 6th structural node (6-y). It will turn out that the data from the dominated node and

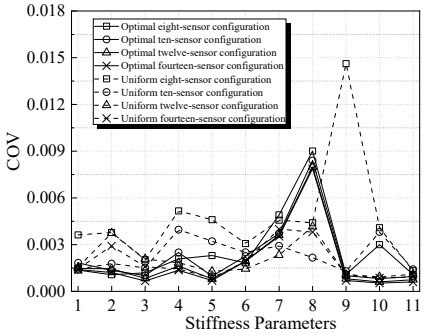

Fig. 8 Resultant COV of the optimal and uniform configurations

sensors at the y-direction of the 4th node (4-y) and the x-direction of the 26th node (26-x) cannot be received. As a result, the associated maximum COV of the parameters increases to 1.58%, which is 1.8 times that of the optimal eight-sensor configuration (0.90%) during the lifespan. To ensure the estimation accuracy, one possible solution is to place a backup sensor at the same location as the dominated node. Once the dominated node run out of the energy, the backup sensor be reassigned as the dominated node. Since the energy of other sensor nodes in the optimal eight-sensor configuration will not be exhausted before the backup sensor runs out of the energy, the lifetime of this configuration can be doubled (3346 h) after using the scheme of placing the backup sensor.

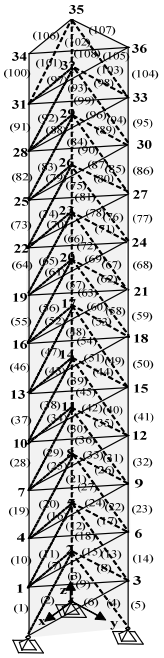

Fig. 9 Space truss model

6.2 Example 2: Space truss model

6.2.1 Multi-type sensory system

In the second example, a space truss model (shown in Fig. 9) with 108 DOFs is considered. The bolded numbers denote the node numbers and the numbers in parenthesis denote the structural member numbers, respectively. The space truss consists of 108 bars with uniform cross section area $A = 0.001\ \mathrm{m}^2$. The structure has a triangular base that spans 20 m in both x-direction and y-direction. The truss has twelve identical layers with the overall height equal to 120 m. The mass density and the modulus of elasticity of the bars are $7850\ \mathrm{kg/m}^3$ and 3×10^{10} Pa, respectively. The first ten nominal natural frequencies are 0.388 Hz, 0.412 Hz, 0.834 Hz, 1.613 Hz, 1.750 Hz, 2.533 Hz, 3.193 Hz, 3.667 Hz, 3.792 Hz and 4.384 Hz. Again, Rayleigh damping model is assumed, i.e., $\mathbf{D} = \varphi_{\mathrm{M}}\mathbf{M} + \varphi_{\mathrm{K}}\mathbf{K}$, where φ_{M} and φ_{K} are $0.0251\ \mathrm{s}^{-1}$ and $3.979 \times 10^{-3}\ \mathrm{s}$, respectively, so that the damping ratios are 1% for the first two modes. The stiffness matrix $\mathbf{K}$ is parameterized with ten parameters $\vartheta_{k1}, \ldots, \vartheta_{k10}$, denoted as: $k_j = \vartheta_{k1},\ j = 1, \ldots, 6$; $k_j = \vartheta_{k2},\ j = 7, \ldots, 9$; $k_j = \vartheta_{k3},\ j = 10, \ldots, 15$; $k_j = \vartheta_{k4},\ j = 16, \ldots, 18$; $k_j = \vartheta_{k5},\ j = 19, \ldots, 27$; $k_j = \vartheta_{k6},\ j = 28, \ldots, 36$; $k_j = \vartheta_{k7},\ j = 37, \ldots, 54$; $k_j = \vartheta_{k8},\ j = 55, \ldots, 72$; $k_j = \vartheta_{k9},\ j = 73, \ldots, 90$; $k_j = \vartheta_{k10},\ j = 91, \ldots, 108$. Therefore, the lower part of the truss has a denser parametrization than the upper part. Two types of commonly used sensors, strain gauges and accelerometers, are installed to monitor the structural response. For both types of sensors, the cluster radius is 30 m, the stored energy of each sensor node is $\varepsilon_0 = 1 \times 10^4$ J, the electronics energy coefficient for data transmission is $\epsilon_T = 45\ \mathrm{nJ/bit}$, the electronics energy coefficient for data reception is $\epsilon_R = 135\ \mathrm{nJ/bit}$, the energy coefficient for data aggregation is $\epsilon_A = 5\ \mathrm{nJ/bit/signal}$, and the rate of bits per packet for strain gauge and accelerometer is $l_s = 3200\ \mathrm{bits/s}$ and $l_a = 4800\ \mathrm{bits/s}$, respectively.

Table 4 Optimal sensor configurations

Case	ξ_r	Strain gauge (No. of member)	Accelerometer (No. of node-direction)
A	1.0%	7,16,47,56,70,75	13-x,14-x,20-x,29-x
	1.5%	10,25,37,47,68,70	4-x,13-z,20-x,26-x
	2.0%	31,38,40,48,69,77	7-z,14-y,20-x,23-z
B	1.0%	7,46,62,74,84	2-x,4-x,6-x,20-x,29-x
	1.5%	20,29,33,74,96	13-z,20-x,23-y,28-y,32-x
	2.0%	15,23,32,58,79	11-x,12-z,18-x,20-x,21-z

Two cases, namely Case A and B, with different constraints on the number of sensors are considered. In Case A, ten sensors with no constraint on the number of sensors for each type. In Case B, ten sensors with five strain gauges and five accelerometers. Table 4 shows the results of the optimal sensor configurations obtained under the required COV threshold of 1.0%, 1.5% and 2.0% for both cases. The second column in the table indicates the required COV threshold of the estimated parameters. The third and the fourth column show the locations of the strain gauges and accelerometers in the optimal design, respectively.

As shown in Table 4, the acceleration response at the x-direction of the 20th node is critical. This measurement is involved in all the optimal sensor configurations regardless the required COV threshold and the sensor constraints. Furthermore, for a given required COV threshold, some common sensors are involved in the optimal configuration of both cases. For example, under the required 1.0% COV threshold, the strain gauge on the 7th member, and the accelerometers in the x-direction of the 20th node and the x-direction of the 29th node are involved in both cases.

The optimal network configurations of Case A and Case B are shown in the Figs. 10 and 11, respectively. The bottom, middle, and top level in the optimal network configurations represent the locations of the non-cluster head nodes, the cluster head nodes, and the base station, respectively. Data is transmitted between the sensors of

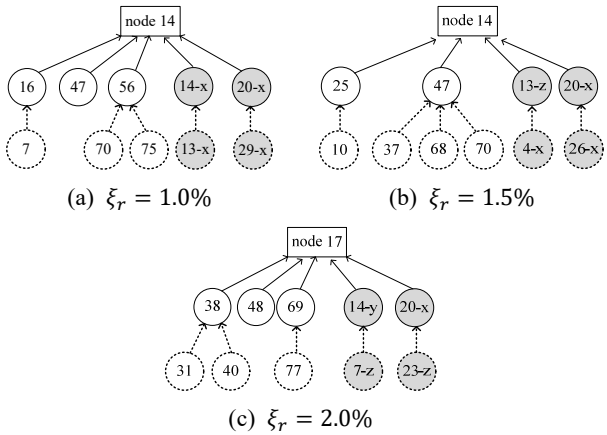

(a) $\xi_r = 1.0\%$ (b) $\xi_r = 1.5\%$

(c) $\xi_r = 2.0\%$

Fig. 10 Optimal network configurations of different required COV threshold of Case A

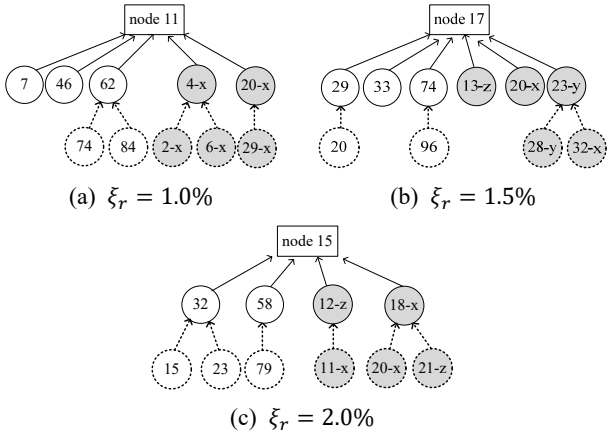

(a) $\xi_r = 1.0\%$ (b) $\xi_r = 1.5\%$

(c) $\xi_r = 2.0\%$

Fig. 11 Optimal network configurations of different required COV threshold of Case B

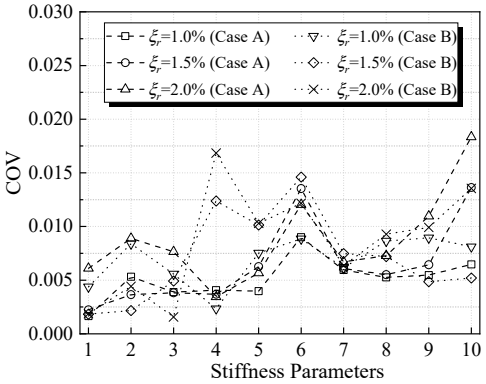

Fig. 12 The resultant COV of the estimated parameters of the optimal configurations

the same type. For the situation that a cluster only contains a sole sensor (e.g., the strain gauge of the 47th structural member shown in Fig. 10(a)), the sensor serves as a cluster head. In Case A, the optimal configurations with the required 1.0%, 1.5% and 2.0% COV threshold has five, four and five clusters, respectively. In Case B, the optimal configurations with the required 1.0% COV threshold contains the same number of clusters as Case A. The optimal configuration has six clusters under the required 1.5% COV threshold while the optimal configuration has four clusters when the required COV threshold is 2.0%.

Fig. 12 shows the resultant COV of the estimated stiffness parameters. It summarizes the results of the optimal sensor configurations obtained under the different required COV threshold. It can be observed that the obtained optimal sensor configurations achieved the required estimation accuracy in both cases. The maximum COV of the estimated stiffness parameters increases as the required COV threshold relaxes. For example, in Case A, the maximum COV of the optimal configuration were lower than the required COV thresholds. In particular, the resultant maximum COV are 0.90%, 1.36% and 1.84% when the required COV threshold are 1.0%, 1.5% and 2.0%, respectively. The result shows that all the optimal designs satisfied the required estimation accuracy.

Table 5 Network rate of energy consumption, dominated node, dominated node rate of energy consumption and lifetime of the optimal configurations

Case	ξ_r	E_{total} (J/h)	Dominated node	$E_{\mathcal{M}}$ (J/h)	L (h)
A	1.0%	32.41	16	13.68	730
	1.5%	26.85	20-x	6.05	1652
	2.0%	20.16	69	4.27	2341
B	1.0%	70.56	20-x	17.28	578
	1.5%	42.48	23-y	8.47	1180
	2.0%	21.24	18-x	5.88	1700

Table 5 shows the network rate of energy consumption, dominated node, dominated node rate of energy consumption and lifetime of the optimal sensor configurations under different required COV thresholds. In both cases, the network rate of energy consumption of the optimal design decreases as the required COV threshold increases. For all the six optimal sensor configurations, the dominated node is a cluster head node in the network. Furthermore, in both cases, the corresponding rate of energy consumption of the dominated node of the optimal design becomes lower when the required estimation accuracy is lower. Therefore, the larger the required COV threshold, the longer the lifetime of the optimal sensor configuration. For example, the lifetime of the optimal configuration of Case A obtained under the required 2% COV threshold is 2341 h, which is more than a double compares to that of the required 1.0% COV threshold. On the other hand, the lifetime of the optimal sensor configuration of Case A is larger than that of Case B under the same required COV threshold. For example, the lifetime of the optimal design of Case A is 152 h longer than that of Case B under the required 1.0% COV threshold. This is because the imposed constrains introduced additional restriction and the configurations do not achieve the required estimation accuracy are eliminated in the optimization.

6.2.2 Validation

In this section, a validation of the effectiveness of the proposed method is presented. The required COV threshold of the estimated parameters is 1.0%. Six configurations with five accelerometers and five strain gauges are utilized for comparison and their sensor locations are shown in Table 6. In particular, the optimal configuration obtained by the proposed method under the specified conditions is denoted as the designed configuration. In Trial 1, the sensors deployed evenly over the structure. In Trial 2, the sensor locations were randomly selected. The sensors of Trial 3, 4 and 5 were placed around the bottom, middle or top part of the structure, respectively. Based on the proposed cluster-based network optimization algorithm, the corresponding network configurations are obtained. With the same fashion as Fig. 10, Fig. 13 summarizes the result of the network configuration. For all the six sensor configurations, the configurations contained at least four clusters. It is found that the configuration of Trial 1 has six clusters which is more than the other concerned

Table 6 Sensor locations for validation

		Strain gauge (No. of member)	Accelerometer (No. of node-direction)
Designed configuration		7,46,62,74,84	2-x,4-x,6-x,20-x,29-x
Trial	1	2,13,49,55,74	7-x,11-x,24-x,28-x,36-x
	2	11,20,83,89,93	9-x,12-x,17-x,19-x,27-x
	3	1,12,20,37,51	1-x,6-x,7-x,11-x,15-x
	4	31,41,49,57,65	10-x,14-x,18-x,19-x,24-x
	5	60,68,80,91,103	21-x,23-x,27-x,28-x,32-x

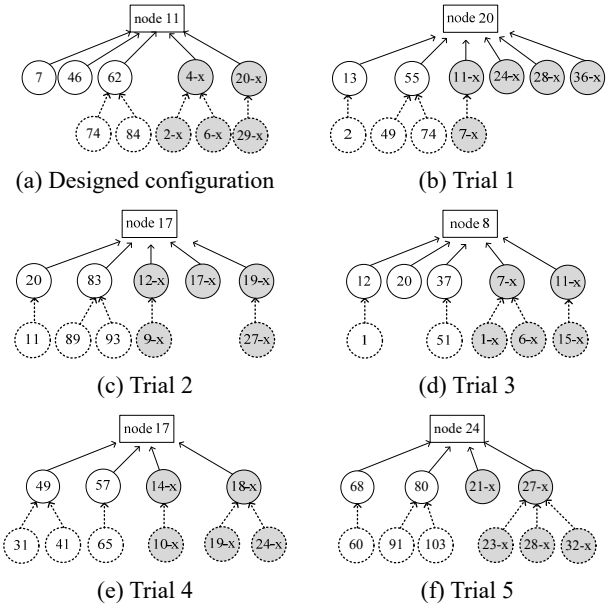

(a) Designed configuration (b) Trial 1

(c) Trial 2 (d) Trial 3

(e) Trial 4 (f) Trial 5

Fig. 13 Network configurations

configurations.

The space truss was subjected to base excitation that modeled as zero-mean Gaussian white noise with spectral intensities $5 \times 10^{-4}\ \mathrm{m^2 s^{-3}}$, $5 \times 10^{-4}\ \mathrm{m^2 s^{-3}}$ and $4 \times 10^{-4}\ \mathrm{m^2 s^{-3}}$ in the x-, y- and z-direction, respectively. The sampling interval was $\Delta t = 0.005\ \mathrm{s}$ and the total monitoring period was 100 s. The measurement noise was taken as 5% of the root-mean-square of the noise-free response.

Table 7 shows the identification results of the ten concerned stiffness parameters and Fig. 14 shows the corresponding COVs. Table 8 shows the lifetime of the six configurations. From Fig. 14, it is found that except for the designed configuration, the maximum COV of the estimated parameters are larger than 1.0%. In particular, the maximum COV of Trial 5 is as high as 4.6%. Furthermore, the lifetime of the designed configuration is 578 h, which is 8.5 times and 1.7 times of that of Trial 1 and 2, respectively. Trial 5 has the longest lifespan among all the concerned configurations. Although the lifetime of Trial 3 to 5 is longer than that of the designed configuration, their estimation accuracy does not fulfill the requirement. The result shows that the optimal designed configuration achieves the required estimation accuracy with the longest lifespan.

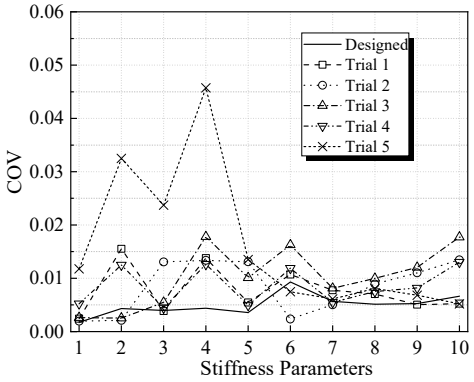

Fig. 14 Resultant COV of the parameters

Table 8 Lifetime of the six configurations

	Designed configuration	Trial 1	Trial 2	Trial 3	Trial 4	Trial 5
L (h)	578	68	332	1495	1653	1702

Table 7 shows the identification results of the ten concerned stiffness parameters and Fig. 14 shows the corresponding COVs. Table 8 shows the lifetime of the six configurations. From Fig. 14, it is found that except for the designed configuration, the maximum COV of the estimated parameters are larger than 1.0%. In particular, the maximum COV of Trial 5 is as high as 4.6%. Furthermore, the lifetime of the designed configuration is 578 h, which is 8.5 times and 1.7 times of that of Trial 1 and 2, respectively. Trial 5 has the longest lifespan among all the concerned configurations. Although the lifetime of Trial 3 to 5 is longer than that of the designed configuration, their estimation accuracy does not fulfill the requirement. The result shows that the optimal designed configuration achieves the required estimation accuracy with the longest lifespan.

7. Conclusions

This paper presented a wireless sensor network configuration optimization method for multi-type wireless sensory system. This method develops the optimal information and lifespan versatile wireless sensor network configuration for structural health monitoring. Based on the Bayesian inference, the COV of the estimated parameters is obtained to evaluate the estimation accuracy of the installed sensors. It provides a holistic measure to quantify the quality of information captured by a wireless sensor network regardless the sensor types and network configuration. A cluster-based network optimization algorithm is developed to determine the longest lifespan of the sensor network. The proposed method was applied to design the optimal wireless sensor network configuration of a cable-stayed bridge and a space truss. The illustrative examples demonstrated that the proposed method provides

the longest lifespan wireless sensor network configuration that satisfies the required estimation accuracy. The results showed that the proposed approach can be widely used for wireless sensor network design regardless of the type of structures and sensors.

Acknowledgments

This work is funded by the Science and Technology Development Fund, Macau SAR under Research Grant SKL-IOTSC(UM)-2021-2023 and 0094/2021/A2, the Research Committee of University of Macau under Research Grant MYRG2018-00048-AAO and SRG2021-00006-FST, and the Guangdong-Hong Kong-Macau Joint Laboratory Program under Grant 2020B1212030009. These generous supports are gratefully acknowledged.

References

Akkaya, K., Younis, M. and Youssef, W. (2007), "Positioning of base stations in wireless sensor networks", *IEEE. Commun. Mag.*, **45**(4), 96-102. https://doi.org/10.1109/MCOM.2007.343618

Al-Turjman, F.M. (2018), "Optimized hexagon-based deployment for large-scale ubiquitous sensor networks", *J. Netw. Syst. Manag.*, **26**(2), 255-283. https://doi.org/10.1007/s10922-017-9415-2

Al-Turjman, F.M., Hassanein, H.S. and Ibnkahla, M. (2015), "Towards prolonged lifetime for deployed WSNs in outdoor environment monitoring", *Ad. Hoc. Netw.*, **24**, 172-185. https://doi.org/10.1016/j.adhoc.2014.08.017

Argyris, C., Papadimitriou, C. and Panetsos, P. (2017), "Bayesian optimal sensor placement for modal identification of civil infrastructures", *J. Smart Cities.*, **2**(2), 69-86. http://dx.doi.org/10.26789/JSC.2016.02.001

Argyris, C., Chowdhury, S., Zabel, V. and Papadimitriou, C. (2018), "Bayesian optimal sensor placement for crack identification in structures using strain measurements", *Struct. Control. Health. Monit.*, **25**(5), e2137. https://doi.org/10.1002/stc.2137

Bhuiyan, M.Z.A. and Cao, J.N. (2015), "Deploying wireless sensor networks with fault-tolerance for structural health monitoring", *IEEE Trans. Comput.*, **64**, 382-395. https://doi.org/10.1109/TC.2013.195

Casciati, F. and Fuggini, C. (2011), "Monitoring a steel building using GPS sensors", *Smart Struct. Syst., Int. J.*, **7**(5), 349-363. https://doi.org/10.12989/sss.2011.7.5.349

Cho, S., Yun, C.B., Lynch, J.P., Zimmerman, A.T., Spencer Jr, B.F. and Nagayama, T. (2008), "Smart wireless sensor technology for structural health monitoring of civil structures", *Steel Struct.*, **8**, 267-275. www.ijoss.org

El-Qawasma, F.A., Elfouly, T.M. and Ahmed, M.H. (2019), "Minimising number of sensors in wireless sensor networks for structure health monitoring systems", *IET. Wireless. Sensor Syst.*, **9**(2), 94-101. https://doi.org/10.1049/iet-wss.2018.5031

Elsersy, M., Elfouly, T.M. and Ahmed, M.H. (2016), "Joint optimal placement, routing, and flow assignment in wireless sensor networks for structural health monitoring", *IEEE Sensors. J.*, **16**(12), 5095-5106. https://doi.org/10.1109/JSEN.2016.2554462

Fang, K., Liu, C. and Teng, J. (2018), "Cluster-based optimal wireless sensor deployment for structural health monitoring", *Struct. Health. Monit.*, **17**(2), 266-278. https://doi.org/10.1177/1475921717689967

Fu, T.S., Ghosh, A., Johnson, E.A. and Krishnamachari, B. (2013), "Energy-efficient deployment strategies in structural health monitoring using wireless sensor networks", *Struct. Control. Health. Monit.*, **20**(6), 971-986. https://doi.org/10.1002/stc.1510

Geoffrine, J.M.C. and Geetha, V. (2019), "Energy optimization with higher information quality for SHM application in wireless sensor networks", *IEEE Sensors J.*, **19**(9), 3513-3520. https://doi.org/10.1109/JSEN.2019.2892870

Gul, M. and Catbas, F.N. (2011), "Structural health monitoring and damage assessment using a novel time series analysis methodology with sensor clustering", *J. Sound Vib.*, **330**(6), 1196-1210. https://doi.org/10.1016/j.jsv.2010.09.024

Heinzelman, W.B., Chandrakasan, A.P. and Balakrishnan, H. (2002), "An application-specific protocol architecture for wireless microsensor networks", *IEEE. Trans. Wirel. Commun.*, **1**, 660-670. https://doi.org/10.1109/TWC.2002.804190

Heredia-Zavoni, E. and Esteva, L. (1998), "Optimal instrumentation of uncertain structural systems subject to earthquake motions", *Earthq. Eng. Struct. Dyn.*, **27**(4), 343-362. https://doi.org/10.1002/(SICI)1096-9845(199804)27:4<343:AID-EQE726>3.0.CO;2-F

Jalsan, K.E., Rohan, N.S. and Flouri, K. (2014), "Layout optimization of wireless sensor networks for structural health monitoring", *Smart Struct. Syst., Int. J.*, **14**(1), 39-54. https://doi.org/10.12989/sss.2014.14.1.039

Jung, H.J., Kim I.H. and Jang, S.J. (2011), "An energy harvesting system using the wind-induced vibration of a stay cable for powering a wireless sensor node", *Smart. Mater. Struct.*, **20**(7), 075001. http://dx.doi.org/10.1088/0964-1726/20/7/075001

Kammer, D.C. (1991), "Sensor placement for on-orbit modal identification and correlation of large space structures", *J. Guid. Control Dyn.*, **14**(2), 251-259. https://doi.org/10.2514/3.20635

Katafygiotis, L.S. and Yuen, K.V. (2001), "Bayesian spectral density approach for modal updating using ambient data", *Earthq. Eng. Struct. Dyn.*, **30**(8), 1103-1123. https://doi.org/10.1002/eqe.53

Kuok, S.C. and Yuen, K.V. (2016), "Investigation of modal identification and modal identifiability of a cable-stayed bridge with Bayesian framework", *Smart Struct. Syst., Int. J.*, **17**(3), 445-470. http://dx.doi.org/10.12989/sss.2016.17.3.445

Kurata, N., Spencer Jr, B.F. and Ruiz-Sandoval, M. (2005), "Risk monitoring of buildings with wireless sensor networks", *Struct. Control. Health. Monit.*, **12**, 315-327. https://doi.org/10.1002/stc.73

Lam, H.F. and Adeagbo, M.O. (2022), "An enhanced sequential sensor optimization scheme and its application in the system identification of a rail-sleeper-ballast system", *Mech. Syst. Signal. Process.*, **163**, 108188. https://doi.org/10.1016/j.ymssp.2021.108188

Lam, H.F., Yuen, K.V. and Beck, J.L. (2006), "Structural health monitoring via measured Ritz vectors utilizing artificial neural networks", *Comput. Aided. Civil Inf. Eng.*, **21**(4), 232-241. https://doi.org/10.1111/j.1467-8667.2006.00431.x

Lam, H.F., Wong, M.T. and Yang, Y.B. (2012), "A feasibility study on railway ballast damage detection utilizing measured vibration of in situ concrete sleeper", *Eng. Struct.*, **45**, 284-298. https://doi.org/10.1016/j.engstruct.2012.06.022

Lam, H.F., Alabi, S.A. and Yang, J.H. (2017), "Identification of rail-sleeper-ballast system through time-domain Markov chain Monte Carlo-based Bayesian approach", *Eng. Struct.*, **140**, 421-436. https://doi.org/10.1016/j.engstruct.2017.03.001

Lam, H.F., Yang, J.H. and Au, S.K. (2018), "Markov chain Monte Carlo-based Bayesian method for structural model updating and damage detection", *Struct. Control. Health. Monit.*, **25**(4), e2140. https://doi.org/10.1002/stc.2140

Lei, Y., Shen, W.A., Song, Y. and Wang, Y. (2010), "Intelligent

wireless sensors with application to the identification of structural modal parameters and steel cable forces: from the lab to the field", *Adv. Civil Eng.*, **2010**, 1-9. https://doi.org/10.1155/2010/316023

Lei, Y., Chen, F. and Zhou, H. (2015), "An algorithm based on two-step Kalman filter for intelligent structural damage detection", *Struct. Control. Health. Monit.*, **22**(4), 694-706. https://doi.org/10.1002/stc.1712

Lei, Y., Yang, N. and Xia, D.D. (2017), "Probabilistic structural damage detection approaches based on structural dynamic response moments", *Smart Struct. Syst., Int. J.*, **20**(2), 207-217. https://doi.org/10.12989/sss.2017.20.2.207

Lei, Y., Lu, J.B. and Huang, J.S. (2020), "Synthesize identification and control for smart structures with time-varying parameters under unknown earthquake excitation", *Struct. Control. Health.* Monit., **27**(4), e2512. https://doi.org/10.1002/stc.2512

Li, B., Wang, D., Wang, F. and Ni, Y.Q. (2010), "High quality sensor placement for SHM systems: Refocusing on application demands", *Proceedings of INFOCOM'10*, *International Conference on IEEE*, San Diego, CA, USA, March.

Li, S.L., Dong, J.L., Lu, W., Lim H., Xu, W.C. and Jin, Y. (2017a), "Optimal sensor placement for cable force monitoring using spatial correlation analysis and bond energy algorithm", *Smart Struct. Syst., Int. J.*, **20**(6), 769-780. https://doi.org/10.12989/sss.2017.20.6.769

Li, J., Hao, H. and Chen, Z. (2017b), "Damage identification and optimal sensor placement for structures under unknown traffic-induced vibrations", *J. Aerosp. Eng.*, **30**(2), B4015001. https://doi.org/10.1061/(ASCE)AS.1943-5525.0000550

Liu, W., Gao, W.C., Sun, Y. and Xu, M.J. (2008), "Optimal sensor placement for spatial lattice structure based on genetic algorithms", *J. Sound Vib.*, **317**, 175-189. https://doi.org/10.1016/j.jsv.2008.03.026

Liu, X., Cao, J., Lai, S., Yang, C., Wu, H. and Xu, Y. (2011), "Energy efficient clustering for WSN-based structural health monitoring", *Proceedings of 30th IEEE International Conference on Computer Communications* (*INFOCOM*), Shanghai, China, April.

Liu, C., Fang, K. and Teng, J. (2015), "Optimum wireless sensor deployment scheme for structural health monitoring: a simulation study", *Smart. Mater. Struct.*, **24**, 115034. https://doi.org/10.1088/0964-1726/24/11/115034

Liu, C., Jiang, Z., Wang, F. and Chen, H. (2016), "Energy-efficient heterogeneous wireless sensor deployment with multiple objectives for structural health monitoring", *Sensors*, **16**, 1865. https://doi.org/10.3390/s16111865

Mak, N.H. and Seah, W.K.G. (2009), "How long is the lifetime of a wireless sensor network?", *Proceedings of International Conference on Advanced Information Networking and Applications*, Bradford, UK, May.

Ni, Y., Wang, Y. and Xia, Y. (2015), "Investigation of mode identifiability of a cable-stayed bridge: comparison from ambient vibration responses and from typhoon-induced dynamic responses", *Smart Struct. Syst., Int. J.*, **15**(2), 447-468. http://dx.doi.org/10.12989/sss.2015.15.2.447

Noori, M., Cao, Y., Hou, Z.K. and Sharma, S. (2010), "Application of support vector machine for reliability assessment and structural health monitoring", *Int. J. Eng. Under. Uncertain.: Hazard. Assess. Mitig.*, **2**(3-4), 89-98.

Onoufriou, T., Soman, R.N., Votsis, R., Chrysostomou, C. and Kyriakides, M. (2012), "Optimization of wireless sensor locations for SHM based on application demands and networking limitations", In: *Management*, *Resilience and Sustainability*: *6th International Conference on Bridge Maintenance*, *Safety and Management*, Stresa, Lake Maggiore, Italy.

Papadimitriou, C. (2004), "Optimal sensor placement methodology for parametric identification of structural systems", *J. Sound Vib.*, **278**(4-5), 923-947. https://doi.org/10.1016/j.jsv.2003.10.063

Papadimitriou, C., Beck, J.L. and Au, S.K. (2000), "Entropy-based optimal sensor location for structural model updating", *J. Vib. Control*, **6**(5), 781-800. https://doi.org/10.1177/107754630000600508

Papadopoulos, M. and Garcia, E. (1998), "Sensor placement methodologies for dynamic testing", *AIAA J.*, **36**(2), 256-263. https://doi.org/10.2514/2.7509

Pei, X.Y., Yi, T.H. and Li, H.N. (2018), "A multitype sensor placement method for the modal estimation of structure", *Smart Struct. Syst., Int. J.*, **21**(4), 407-420. https://doi.org/10.12989/sss.2018.21.4.407

Raich, A.M. and Liszkai, T.R. (2012), "Multi-objective optimization of sensor and excitation layouts for frequency response function-based structural damage identification", *Comput. Aided. Civ. Inf. Eng.*, **27**(2), 95-117. https://doi.org/10.1111/j.1467-8667.2011.00726.x

Reynier, M. and Abou-Kandil, H. (1999), "Sensors location for updating problems", *Mech. Syst. Signal. Process.*, **13**(2), 297-314. https://doi.org/10.1006/mssp.1998.1213

Sengupta, S., Das, S. and Nasir, M.D. (2013), "Multi-objective node deployment in WSNs: In search of an optimal trade-off among coverage, lifetime, energy consumption, and connectivity", *Eng. Appl. Artif. Intell.*, **26**(1), 405-416. https://doi.org/10.1016/j.engappai.2012.05.018

Shi, Q., Wang, X., Chen, W. and Hu, K. (2020), "Optimal sensor placement method considering the importance of structural performance degradation for the allowable loadings for damage identification", *Appl. Math. Model.*, **86**, 384-403. https://doi.org/10.1016/j.apm.2020.05.021

Spencer, B.F., Hoskere, V. and Narazaki, Y. (2019), "Advances in computer vision-based civil infrastructure inspection and monitoring", *Engineering*, **5**(2), 199-222. https://doi.org/10.1016/j.eng.2018.11.030

Stephan, C. (2012), "Sensor placement for modal identification", *Mech. Syst. Signal. Process.*, **27**, 461-470. https://doi.org/10.1016/j.ymssp.2011.07.022

Udwadia, F.E., (1994), "Methodology for optimal sensor locations for parameters identification in dynamic systems", *J. Eng. Mech.*, **120**(2), 368-390.

Wang, A., Heinzelman, W., Sinha, A. and Chandrakasan, A. (2001), "Energy-scalable protocols for battery-operated microsensor networks", *VLSI. Signal. Process.*, **29**, 223-237. https://doi.org/10.1109/SIPS.1999.822354

Wong, K.Y. (2004), "Instrumentation and health monitoring of cable-supported bridges", *Struct. Control. Health.*, **11**(2), 91-124. https://doi.org/10.1002/stc.33

Yao, L., Sethares, W.A. and Kammer, D.C. (1993), "Sensor placement for on-orbit modal identification via a genetic algorithm", *AIAA J.*, **31**(10), 1922-1928. https://doi.org/10.2514/3.11868

Ye, S. and Ni, Y.Q. (2012), "Information entropy based algorithm of sensor placement optimization for structural damage detection", *Smart Struct. Syst., Int. J.*, **10**(4-5), 443-458. https://doi.org/10.12989/sss.2012.10.4_5.443

Yi, T.H. and Li, H.N. (2012), "Methodology developments in sensor placement for health monitoring of civil infrastructures", *Int. J. Distrib. Sens. Netw.*, **8**(8), 612726. https://doi.org/10.1155/2012/612726

Yi, T.H., Li, H.N. and Gu, M. (2013), "Recent research and applications of GPS-based monitoring technology for high-rise structures", *Struct. Control. Health. Monit.*, **20**(5), 649-670. https://doi.org/10.1002/stc.1501

Yi, T.H., Li, H.N. and Zhang, X.D. (2015), "Sensor placement optimization in structural health monitoring using distributed

monkey algorithm", *Smart. Struct. Syst.*, *Int. J.*, **15**(1), 191-207. https://doi.org/10.12989/sss.2015.15.1.191

Yi, T.H., Li, H.N. and Wang, C.W. (2016), "Multiaxial sensor placement optimization in structural health monitoring using distributed wolf algorithm", *Struct. Control. Health. Monit.*, **23**(4), 719-734. https://doi.org/10.1002/stc.1806

Yi, T.H., Huang, H.B. and Li, H.N. (2017), "Development of sensor validation methodologies for structural health monitoring: A comprehensive review", *Measurement*, **109**, 200-214. https://doi.org/10.1016/j.measurement.2017.05.064

Yuen, K.V. and Katafygiotis, L.S. (2005), "An efficient simulation method for reliability analysis of linear dynamical systems using simple additive rules of probability", *Probabilistic. Eng. Mech.*, **20**(1), 109-114. https://doi.org/10.1016/j.probengmech.2004.07.003

Yuen, K.V. and Kuok, S.C. (2015), "Efficient Bayesian sensor placement algorithm for structural identification: a general approach for multi-type sensory systems", *Earthq. Eng. Struct. Dyn.*, **44**(5), 757-774. https://doi.org/10.1002/eqe.2486

Yuen, K.V., Shi, Y.-F., Beck, J.L. and Lam, H.F. (2007), "Structural Protection Using MR Dampers with Clipped Robust Reliability-based Control", *Struct. Multidiscipl. Optimiz.*, **34**(5), 431-443. https://doi.org/10.1007/s00158-007-0097-3

Yuen, K.V., Hao, X.H. and Kuok, S.C. (2022), "Robust sensor placement for structural identification", *Struct. Control. Health. Monit.*, **29**(1), e2861. https://doi.org/10.1002/stc.2861

Zhang, F.L., Ni, Y.Q., Ni, Y.C. and Wang, Y.W. (2016), "Operational modal analysis of Canton Tower by a fast frequency domain Bayesian method", *Smart Struct. Syst.*, *Int. J.*, **17**(2), 209-230. https://doi.org/10.12989/sss.2016.17.2.209

Zhang, J., Maes, K., De Roeck, G., Reynders, E., Papadimitriou, C. and Lombaert, G. (2017), "Optimal sensor placement for multi-setup modal analysis of structures", *J. Sound Vib.*, **401**, 214-232. https://doi.org/10.1016/j.jsv.2017.04.041

Zhao, Y., Noori, M., Altabey, W.A. and Beheshti-Aval, S.B. (2018), "Mode shape-based damage identification for a reinforced concrete beam using wavelet coefficient differences and multiresolution analysis", *Struct. Control. Health. Monit.*, **25**(1), e2041. https://doi.org/10.1002/stc.2041

Zhou, G.D. and Yi, T.H. (2013), "Recent developments on wireless sensor networks technology for bridge health monitoring", *Math. Probl. Eng.*, **3**, 1-33. https://doi.org/10.1155/2013/947867

Zhou, G.D., Yi, T.H. and Zhang, H. (2015), "Energy-aware wireless sensor placement in structural health monitoring using hybrid discrete firefly algorithm", *Struct. Control. Health. Monit.*, **22**, 648-666. https://doi.org/10.1002/stc.1707